Indian Journal of Engineering & Materials Sciences
Vol. 12, December 2005, pp. 487-497

CFD study of isothermal flow in an afterburner system

S Ganesan[a], S Kishore Kumar[a] & V Ganesan[b]

[a]Gas Turbine Research Establishment, Bangalore 560 093, India

[b]Department of Mechanical Engineering, Indian Institute of Technology Madras, Chennai 600 036, India

Received 27 July 2004; accepted 28 July 2005

This paper focuses a detailed numerical prediction of non-reacting flow analysis in a practical 1/3 scaled model gas turbine afterburner system. The analysis is performed using SIMPLE algorithm in a body-fitted multi-block grid using STAR-CD software. The turbulence is simulated using standard k-ε model. The validation of software is carried out in a afterburner model by comparing axial, radial and circumferential velocities at various axial locations. The agreement between the prediction and experimental data are quite reasonable. The analysis is extended to the flow in a practical afterburner system. The afterburner system consists of an annular diffuser, a complex three-dimensional flame stabilizer, a liner with chute, screech and cooling rings holes and a convergent nozzle. The wall static pressures are compared with experimental data obtained from rig results for both core and bypass casing. The agreement between CFD prediction and experimental data are in close agreement. The predicted length of the re-circulation zone of the lower radial gutter is larger (2.7 times width of the gutter) than upper radial gutter, which is about 2.3 times width. This is due to combined effect of annular diffuser and lower radial gutter. But the length of the re-circulation zone of the annular ring is slightly less than (0.94 times) the width of the v-gutter. The effect of different mass flow rates on the afterburner performance is also evaluated and it is observed that mass flow rate does not affect the re-circulation zone characteristics. An increase of 20% in mass flow rate increases the exit nozzle velocity by 35%.

IPC Code: F15D

Many military aircrafts require higher thrust for short duration during operations such as take-off, climb, acceleration and combat manoeuvres. Afterburner provides a light and mechanically simple means of achieving thrust augmentation. The performance of the afterburner is governed by internal aerodynamics and for which proper understanding of the flow characteristics is essential for arriving at an optimum design of the afterburner. Low bypass gas turbine engine afterburner systems are very complex both in geometry and flow behaviour. A typical afterburner will have geometrical complexities such as diffuser, liner with mixing holes along its length and v-gutters. The liner will have different types of orifices for reasons like increasing the level of oxygen of the core flow, for suppressing the noise level and for cooling the liner itself. In a bypass engine, the two streams of different pressures and temperatures are mixed through the holes of liner. The v-gutter, placed in the core flow to anchor the flame, will create turbulence in the mixed flow and also provide conducive environment for flame stabilization.

Extensive experimental and numerical studies behind bluff body flame stabilizers have been carried out in the past. The experimental work of Fuji *et al.*[1,2], Taylor and Whitelaw[3], Yang *et al.*[4] provided a comprehensive review on flow of behind bluff bodies and provided some useful data to validate numerical solutions. However, they were restricted to simple bluff bodies like cone, disk wedge and single v-gutter. Issac *et al.*[5] and Ravichandran[6] studied the flow behaviour of complex three-dimensional flame stabilizers. Many researchers[7–9] investigated numerically the flow behind the simple bluff bodies. Recently, Raffoul *et al.*[10] conducted an experimental and numerical investigation to study the turbulent velocities and stresses behind a two-dimensional bluff body.

In this paper, computational fluid dynamics (CFD) study of the three-dimensional non-reacting flow field in an afterburner is carried out. The numerical tool used for the CFD analysis is the STAR-CD software[11]. The validation of the code is carried out with experimental data of Ravichandran[6] in a model afterburner. The flow analysis is then extended to study the flow behaviour in a practical afterburner system. The effect of different mass flow rates on the afterburner performance has been evaluated.

Geometry and Computational Details

Geometry

Fig. 1a is a schematic of the afterburner considered for analysis. Hot vitiated core gases from low pressure turbine enter the annulus of the exhaust diffuser having nine struts at the inlet and four manifolds and complex assembly of v-gutters having twelve outer arms, six inner arms and one annulus ring. Fig. 1b shows the v-gutter geometry. Cold air enters through the bypass duct and mixes with the hot core flow through chute, screech, and cooling holes located along the liner that separates the core and bypass streams. The annulus opening at the end of the liner permits the rest of the cooling air from the bypass to flow over the variable area convergent nozzle located at the end of the jet pipe.

Sector model and grid

Due to symmetry in the geometry, it is sufficient to model a 60° sector, which includes two outer v-gutters and one inner v-gutter. Fig. 2a shows the sector model of the afterburner along with grid and Fig. 2b shows the sector model of the v-gutter. The various sub components, viz., struts, fuel manifolds and linkages are excluded in the present analysis. Liner thickness is very small as compared to the geometry of the afterburner system. So the liner is assumed to have zero thickness. Since the holes in the liner are very small compared to the overall geometry of the afterburner, porous medium approach is used to model the chute, screech and cooling ring holes. Three grids consisting of 210000, 330000 and 440000 cells are considered for the grid independence study. It is seen that 330000 cells were reasonable for the present model.

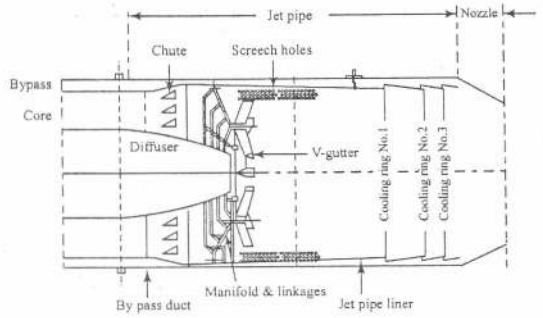

Fig. 1a— Afterburner geometry

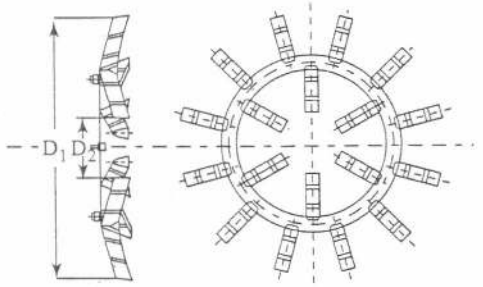

Fig. 1b— V-gutter geometry

Governing Equations

In the present study, the flow in the afterburner system is assumed to be steady, turbulent and compressible. The Reynolds-averaged continuity, momentum and enthalpy equations governing the three-dimensional turbulent flow can be written in Cartesian form as follows.

Continuity equation

$$\frac{\partial}{\partial x_i}[\rho U_i]=0 \qquad \ldots(1)$$

Momentum equations

$$\frac{\partial}{\partial x_i}\left[\rho\, U_j\, U_i\right]=-\frac{\partial p}{\partial x_i}+\frac{\partial \tau_{ij}}{\partial x_j} \qquad \ldots(2)$$

where the turbulent shear stress is given by:

$$\tau_{ij}=-(\mu+\mu_t)\left[\frac{\partial U_i}{\partial x_j}+\frac{\partial U_j}{\partial x_i}\right]-\frac{2}{3}\rho\, k\, \delta_{ij} \qquad \ldots(3)$$

The turbulent viscosity μ_t is obtained by assuming that it is proportional to the product of turbulent velocity scale and length scale.

Energy equation

$$\frac{\partial}{\partial x_i}(\rho\, U_i\, h)=\frac{\partial}{\partial x_i}\left(k\frac{\partial T}{\partial x_i}\right)+U_i\frac{\partial p}{\partial x_i}+\tau_{ij}\frac{\partial U_i}{\partial x_j} \qquad \ldots(4)$$

Turbulence model

In the present study, the two-equation (k-ε) turbulence model which is based on the generalized Boussinesq eddy viscosity concept is employed. This model employs two partial differential equations to estimate the turbulent velocity and length scales and hence is commonly known as two-equation model. The Reynolds stresses in this model are given by

$$-\rho\overline{u_i u_j}=\mu_t\left(\frac{\partial U_i}{\partial x_j}+\frac{\partial U_j}{\partial x_i}\right)-\frac{2}{3}\delta_{ij}\rho\, k \qquad \ldots(5)$$

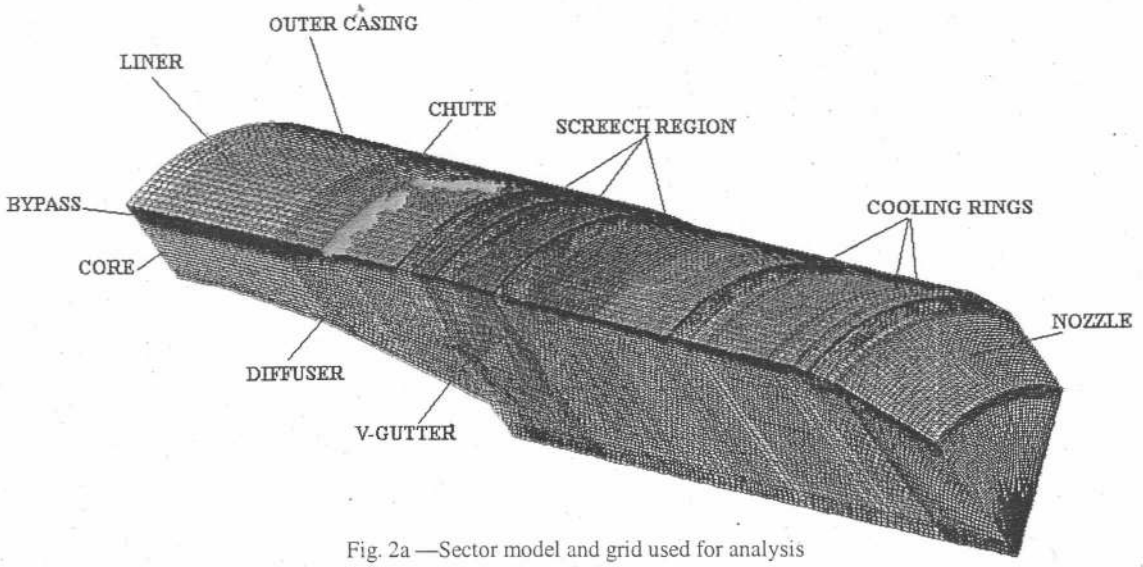

Fig. 2a —Sector model and grid used for analysis

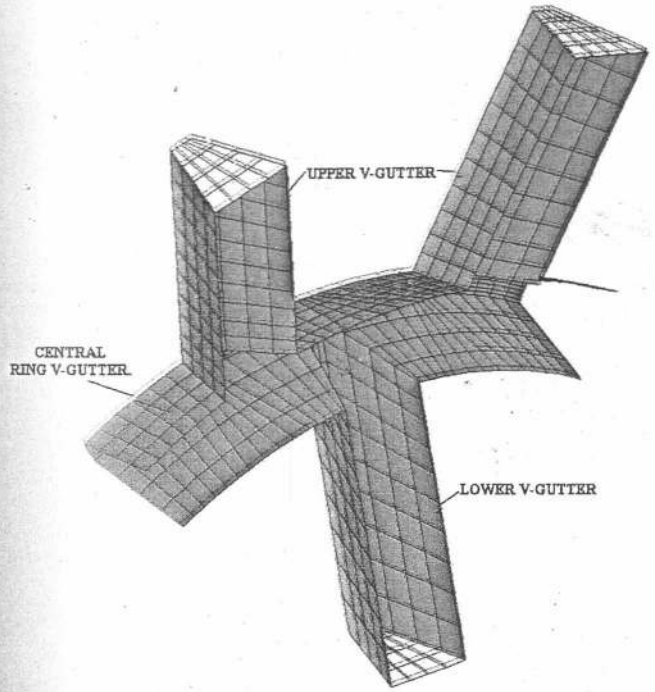

Fig. 2b— Grid in the v-gutter region

The μ_t is the turbulent viscosity that may be related to the kinetic energy of turbulence (k) and its dissipation rate (ε) by dimensional analysis. Thus,

$$\mu_t = C_\mu \rho k^2/\varepsilon \qquad \ldots(6)$$

where C_μ = 0.09. The two-differential equations, which govern the transport of turbulent kinetic energy, k and its dissipation rate, ε are given by,

$$\frac{\partial}{\partial x_j}\left(\rho U_j k\right) = \frac{\partial}{\partial x_j}\left[\left((\mu_l + \mu_t)/\sigma_k\right)\frac{\partial k}{\partial x_j}\right]$$

Table 1 – Inlet conditions

	Total pressure (bar)	Total temperature (K)	Turbulence intensity (%)
Core	2.907	902	10
Bypass	3.174	374	5

$$-\rho\overline{u_i u_j}\frac{\partial U_i}{\partial x_j} - \rho\varepsilon \qquad \ldots(7)$$

$$\frac{\partial}{\partial x_j}\left(\rho U_j \varepsilon\right) = \frac{\partial}{\partial x_j}\left[\left((\mu_l + \mu_t)/\sigma_\varepsilon\right)\frac{\partial \varepsilon}{\partial x_j}\right]$$

$$-C_1\frac{\varepsilon}{k}\rho\overline{u_i u_j}\frac{\partial U_i}{\partial x_j} - C_2\rho\varepsilon^2/k \qquad \ldots(8)$$

where C_1 = 1.44 and C_2 = 1.92 are constants in this model. Moreover the turbulence Prandtl numbers for κ and ε are given by $\sigma_k = 1.0$ and $\sigma_\varepsilon = 1.3$, respectively.

Boundary conditions

At inlet, total pressure, total temperature, turbulence intensity and its scale are specified for both core and bypass region. The various inlet conditions used are shown in Table 1. At the outlet, a uniform static pressure is specified. A wall function approach is used at all solid walls and v-gutter. The axis of the 60°-sector model was assigned symmetry

condition. Cyclic boundary conditions are applied at 0° and 60°-sector.

Results and Discussion

Validation of the code

As a validation exercise of the code STAR-CD, first computations were carried out in an afterburner model for which the experimental data is available. The model afterburner geometry used by Ravichandran[6] is shown in Fig. 3. The model has been fabricated from Perspex and comprises of a cylindrical pipe (200 mm bore and 3 mm wall thickness) and a flame stabilizer of 1 mm thickness. The flame stabilizer is a single ring v-gutter with twelve outer and six inner radial v-gutters and all of them are of width 12 mm (including 2 mm wall thickness), included angle of 40° and creating a blockage of 35%. It is located 50 mm from the test section entry. The overall Reynolds number based on the bulk mean velocity at the entry of the test section and the internal diameter was of the order of 1.3×10^5 and mass flow rate of 0.35 kg/s.

As the geometry of the cylindrical portion repeats itself every 60°, only a single sector of 60° is considered for the present analysis, which includes two outer v-gutters and one inner v-gutter. The grids consisting of 80,000, 150000 and 216000 cells are considered for the present analysis. It is found that the maximum error in axial velocity is less 3% between 150000 and 216000 cells. Hence, the grid of 150000 cells is considered as appropriate, which indicates the grid independent study for this problem.

The mean axial, radial and tangential velocity profiles are compared with experimental values of Ravichandran[6] in the 30° plane (i.e. in the lower v-gutter along with central ring plane) at various axial distances of (X = 70, 80, 90, 100, 120 and 240 mm) from the test section origin. The radial coordinates have been non-dimensionalised using the inner radius of the pipe 100 mm and the velocity normalized using the bulk mean velocity U_o, which is the average axial velocity at the inlet of the test section (9.81 m/s).

Figs 4 a, b and c show the normalized velocity profiles of axial, radial and tangential velocities at 30° plane. It may be observed from Fig. 4a that in general the agreement for axial velocity profiles are good. However, Figs 4b and c show same deviation at X/R = 0.7. It may be noted that X/R = 0.7 is close to the outlet of the gutter and at this section there will be vortex shedding and the flow become unstable. Therefore, capturing accurate data by experimental means is quite difficult. Hence, there is bound to be some deviation at this station. However, as could be seen, at all other stations agreement is quite satisfactory.

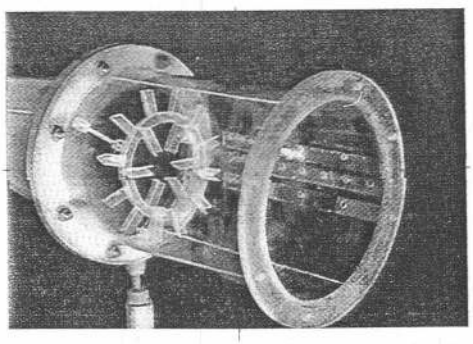

Fig. 3— Afterburner model

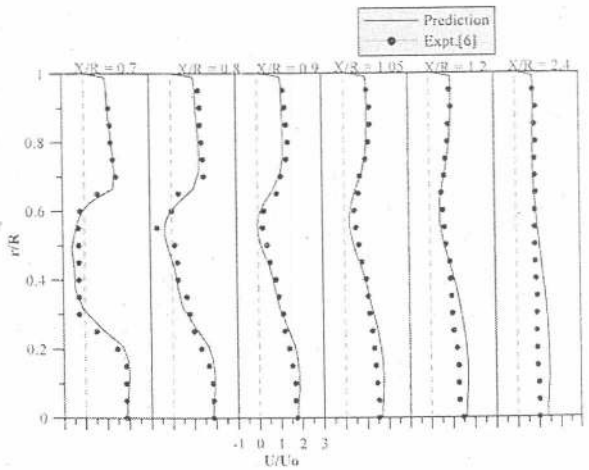

Fig. 4a— Radial variation of axial velocity at 30° plane

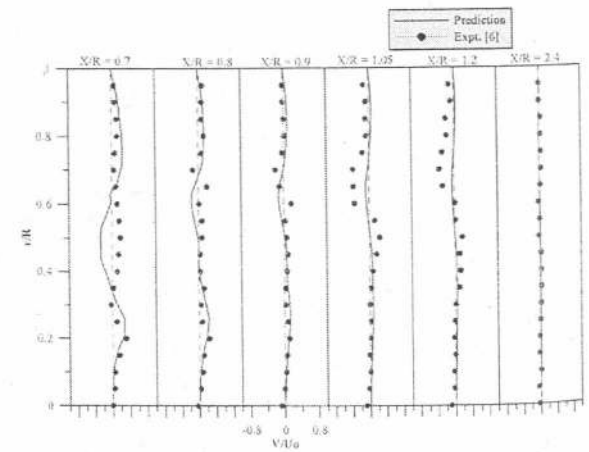

Fig. 4b — Radial variation of radial velocity at 30° plane

Since the flow through the afterburner system is three-dimensional and highly complex, results at different sections are presented for clarity and completeness. Planes at angles 15° and 45° contain the two radial outer gutters, the plane at 30° houses the inner radial gutter and other planes contain only central ring gutter. It is deemed sufficient to restrict attention to only θ = 0°, 15° and 30° planes as these characterize the details of three-dimensionality sufficiently. Fig. 5 shows the different planes of interest.

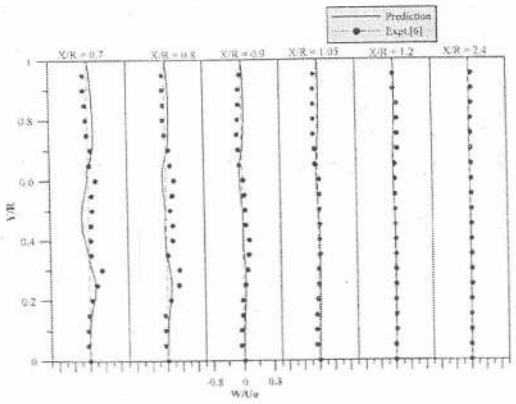

Fig. 4c— Radial variation of tangential velocity at 30° plane

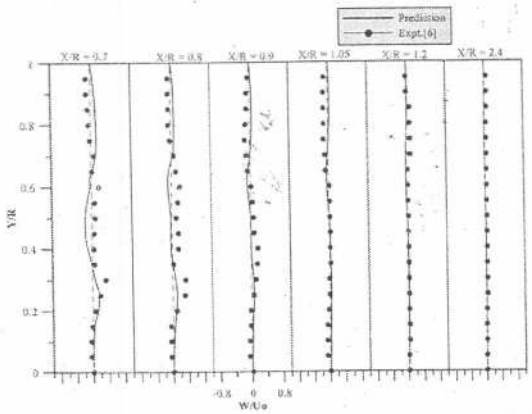

Fig. 5— Sectional view of the model

Velocity vectors

The velocity vector plot in an axial plane (θ = 0°) is shown in Fig. 6a. The flow in the core region starts with a velocity of 330 m/s at the entrance and diffuses to an average velocity of 162 m/s at the end of the diffuser. It can be seen that the flow diffusion is without any flow separation either on the inner or on the outer wall of the diffuser. The flow then enters the v-gutter zone and forms a re-circulation zone around g gutter. The length of the re-circulation zone is less than (0.94 times) the width of the v-gutter. The length of re-circulation gives an indication about the anchoring of the flame. As can be seen flow

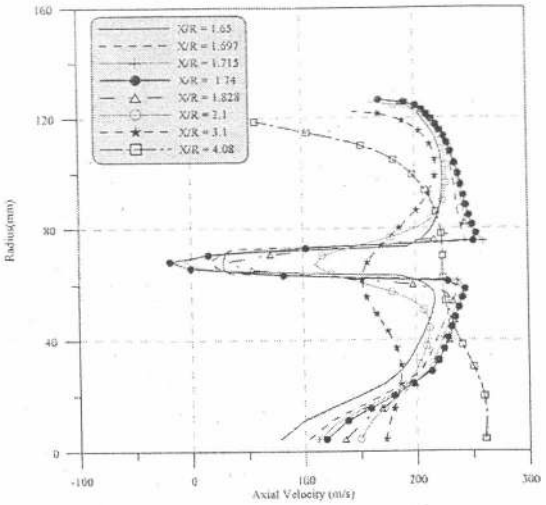

Fig. 6b— Radial variation of axial velocity downstream of the ring gutter at θ = 0° plane

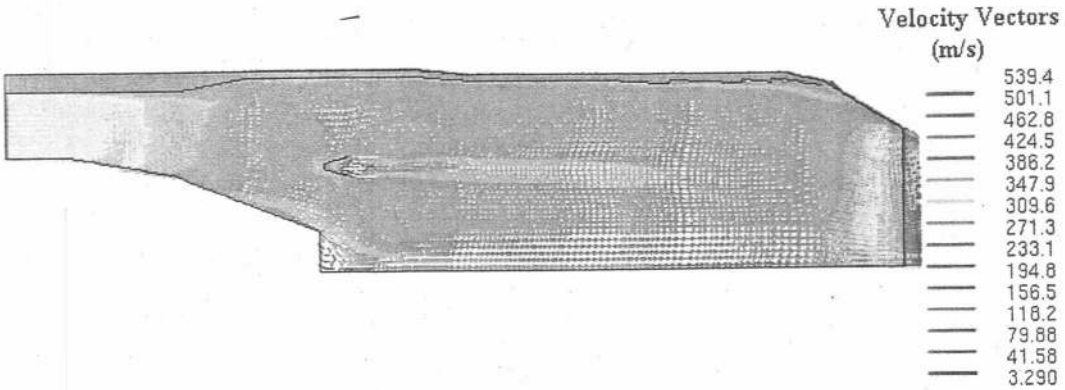

Fig. 6a —Velocity vectors at θ = 0° plane

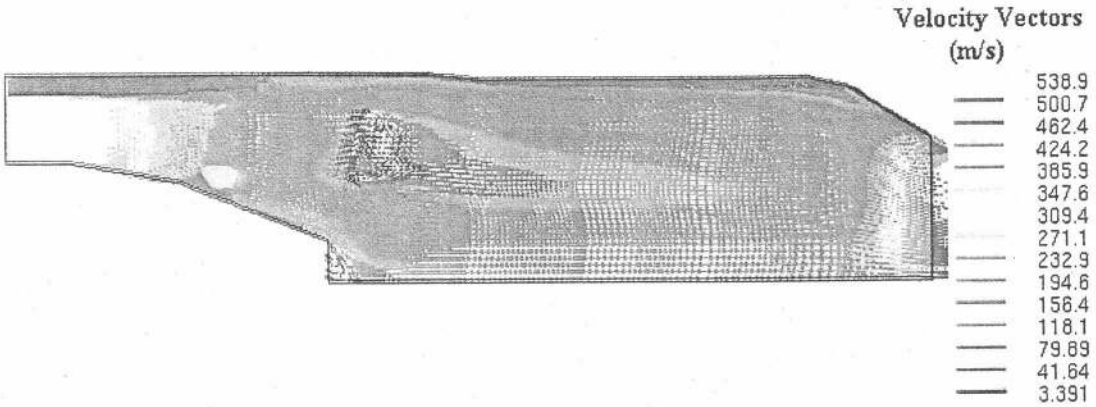

Fig. 7a —Velocity vectors at θ = 15° plane

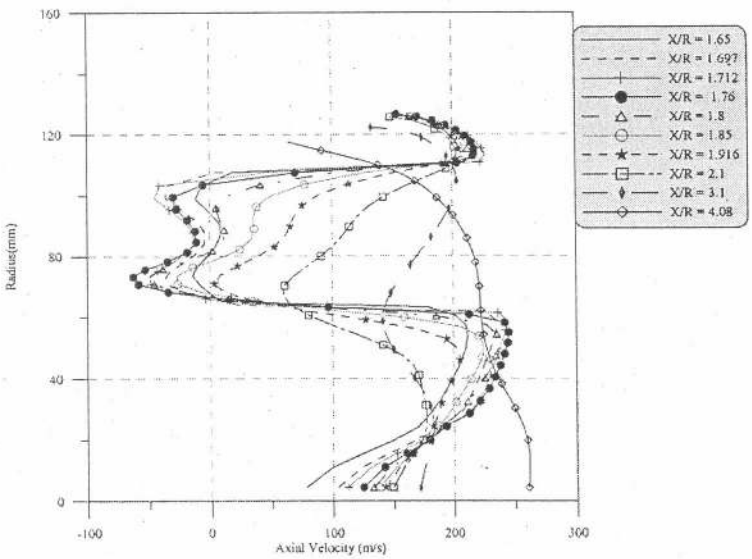

Fig. 7b— Radial variation of axial velocity downstream of the ring gutter at θ = 15° plane

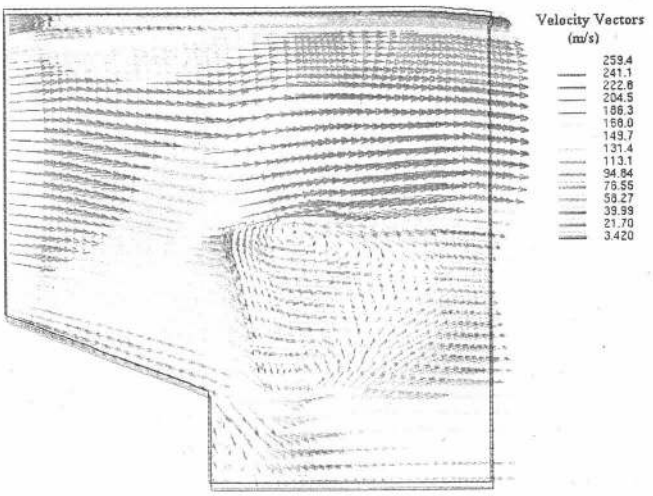

Fig. 8a —Velocity Vectors near ring gutter at θ = 30° plane

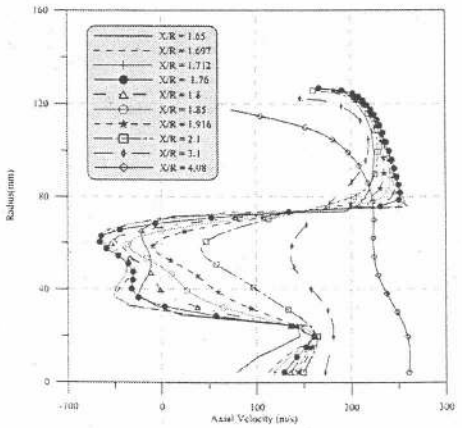

Fig. 8b— Radial variation of axial velocity downstream of the ring gutter at θ = 30° plane

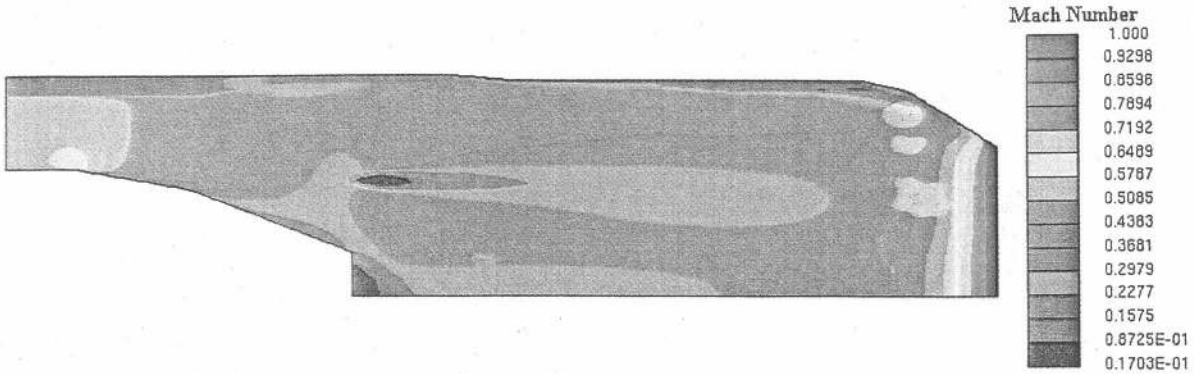

Fig. 9 — Mach number distributions at θ = 0° plane

Fig. 10 —Turbulence kinetic energy distributions at θ = 0° plane

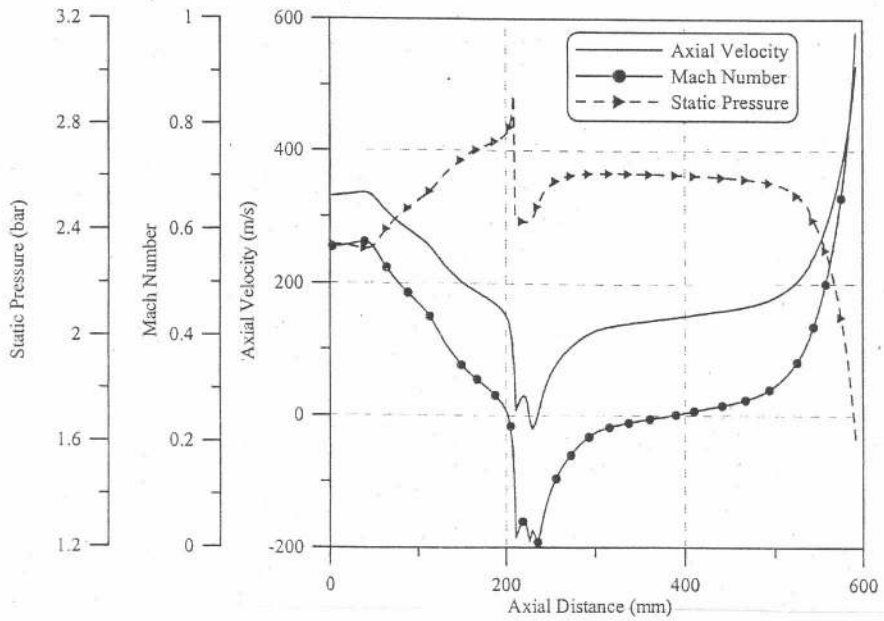

Fig. 11— Variation of Mach number, axial velocity and static pressure along the centre line of the ring gutter at θ = 0° plane

accelerates in the lower and upper side of the ring gutter due to the blockage effect. The flow field details behind the v-gutter are shown in Fig. 6b in terms of radial variation of the axial velocity downstream of the v-gutter. The ring gutter produces a clear re-circulation zone closely behind the v-gutter which can be observed at X/R=1.74. The re-circulation zone (negative velocity) extends radially from r = 65.3 mm to r = 69.5 mm with the negative velocity magnitude peaking to a value of –19.07 m/s at r = 68.3 mm. With further increase in distance, the width of the re-circulation zone reduces and the flow from the two trailing edges of the gutter mix up well, which causes the negative velocity totally disappear at X/R=1.78. The flow velocity increase downstream of the v-gutter and further gets accelerated in the nozzle.

The flow in the bypass region starts with a velocity of 70 m/s at the entrance and accelerates to an average velocity of 131 m/s due to reduction in area near the chutes. The amount of the bypass flow entering into the core flow through chute is 30.3%. The amount of the bypass flow entered into the core flow through screech region is about 28.8%. Further, the bypass flow passes through cooling rings and the amount of the bypass flow entering in the core flow from the cooling rings is 3.9%. Rest of the mass flow (37%) after the third cooling ring mixes with the core flow in the nozzle. The flow accelerates in the nozzle and exits at a velocity of about 540 m/s.

Fig. 7a shows the velocity vectors in the plane (θ = 15°) containing upper radial gutter. The flow behaviour in the diffuser is similar to that of θ = 0° plane. But the combined effect of both ring and upper radial gutter produces a large re-circulation zone, which provides a long shear layer through which burnt and un-burnt products exchange. The axial length of the re-circulation region is about 2.3 times the width of the gutter. The flow field details behind the v-gutter are shown in Fig. 7 b, which shows the radial variation of the axial velocity downstream of the v-gutter. It can be observed from Fig. 7b that there is a large re-circulation zone in the region between r = 66.6 to 104 mm with high negative velocity of -62.7 m/s. This is due to the open portion of the ring gutter in that region which makes better flame spreading characteristics when combustion is on. Although the flow pattern near the v-gutter differs, the nozzle region indicates a similar flow pattern as θ = 0° plane.

Fig. 8a shows the velocity vectors around the lower radial gutter at θ = 30° plane. In this plane, the velocity vector is shown only around the v-gutter region because the flow properties are similar to that of other two planes. A general observation is that the axial length re-circulation is larger (2.7 times width of the gutter) than θ = 15° plane. This is due to combined effect of diffuser and v-gutter. Otherwise the flow behaviour is similar to θ = 15° plane. The flow characteristics behind the v-gutter are shown in Fig. 8b, which shows the radial variation of the axial velocity downstream of the v-gutter. The wake characteristics are similar to θ = 15° plane except there is shift to the lower side of the afterburner.

Mach number distribution

Fig. 9 shows Mach number distribution at θ = 0° plane. The core flow diffuses from 0.507 Mach at the inlet to 0.29 Mach at the end of the diffuser and the Mach number reaches a value of 0.36 at the lip of the v-gutter where the blockage is maximum. The Mach number behind the v-gutter is very small due to wakes of v-gutter and then starts increasing from there towards the nozzle.

The flow in the bypass region enters at a Mach number of 0.18 and accelerates to a Mach number of 0.33 after the chute region. The Mach number in the screech region is about 0.26 and is about 0.12 in the cooling ring regions. The bypass flow then mixes with core flow in the nozzle region and the mixed flow exits at a Mach number of 1.0, which is a choked condition. A similar behaviour is observed at θ = 15° plane and θ = 30° plane expect near the v-gutter.

Turbulent kinetic energy distribution

The turbulent kinetic energy at θ = 0° plane is shown in Fig. 10. The turbulent kinetic energy increases rapidly in the downstream of the gutter resulting in a maximum turbulence kinetic energy in the region as compared with other regions. The regions of high turbulence kinetic energy indicate zones of high mixing and can be expected to be major zones of combustion. It is observed that there is high turbulence kinetic energy in the region in the θ = 15° and θ = 30° plane as compared to the θ = 0° plane which will provide large combustion zone region.

Static pressure distribution

Fig. 11 shows the variation of axial velocity, mach number and static pressure along the axial direction and at the centre line of ring gutter (R = 68 mm). It can be seen that the effect of reduction in velocity in

the diffuser is compensated by the increase in static pressure in the diffuser. The static pressure is seen increasing from 2.35 bar at entrance to 2.723 bar at end of the diffuser. Then the static pressure is seen decreasing to a value of 2.5 bar at gutter back surface. Again in the nozzle the static pressure is seen reducing as the velocity in that portion increases.

The diffuser static pressure recovery co-efficient (C_p) of 0.657 and the diffuser efficiency of 93.4% is obtained from the following relation.

$$\text{Diffuser efficiency} = \eta = \frac{C_{p-actual}}{C_{p-ideal}} * 100$$

$$\text{where } C_{p-actual} = \frac{P_2 - P_1}{P_{01} - P_1} \quad \text{and}$$

$$C_{p-ideal} = 1 - \left(\frac{A_1}{A_2}\right)^2$$

Total pressure loss

The predicted total pressure loss in the core region up to diffuser end is 1.3% and is about 4.83% in the core region from inlet to core end. The loss in the bypass region is 6.12%. The actual total pressure loss in the practical afterburner might be higher than predicted here due to non-inclusion of struts, fuel manifolds and linkages.

Comparison with rig results

The predicted wall static pressures are compared with experimental data obtained from the rig test. Fig. 12 shows the wall static pressure in the core and outer casing of the afterburner. Reasonably good agreements are obtained between the CFD analysis and rig results.

Effect of mass flow rate

A parametric study has been carried out by varying the inlet mass flow rate which represents design and different off-design conditions of engine operation. Fig. 13a shows the radial variation of the axial velocity profile at the end of the exhaust diffuser at θ=30° plane. It can be seen from the Fig. 13a that as the mass flow rate increases the diffuser exit axial velocity increases which leads to a an increase in total pressure loss in the diffuser. Fig. 13b shows the total pressure loss and diffuser efficiency with mass flow rate. With the increase in mass flow rate from 6.7 kg/s to 8.38 kg/s, a marginal increase in the diffuser efficiency is obtained from 91% to 93.4% with pressure recovery coefficient of 0.64 to 0.657. Hence, it can be seen that the performance of the diffuser is satisfactory.

Fig. 13c shows the radial variations of axial velocity profile just behind the v-gutter at x = 1.76 at the θ=30° plane. It can be seen from the Fig. 13c that there is no change in velocity magnitude in the re-circulation zone with increasing mass flow rate. This indicates that the axial length and width of the re-circulation zone is same with mass flow rate. But there is an increase in axial velocity in the lower and upper side of the v-gutter region. The velocity variation away from the re-circulation zone at a distance of x/r = 2.66 is shown in Figs 13d and e shows at the entry of the nozzle. Here a marginal increase in velocity is obtained with mass flow rate.

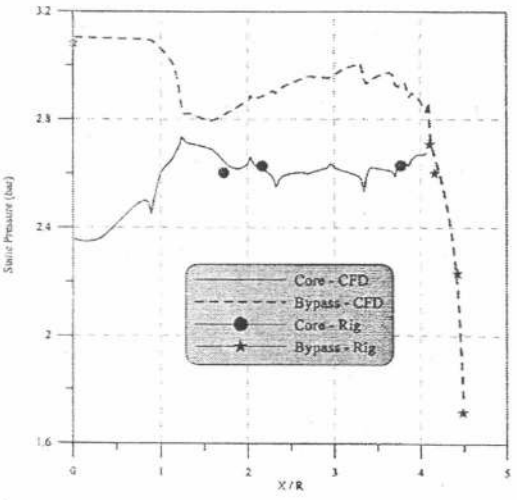

Fig. 12 — Wall static pressure in the core and outer casing

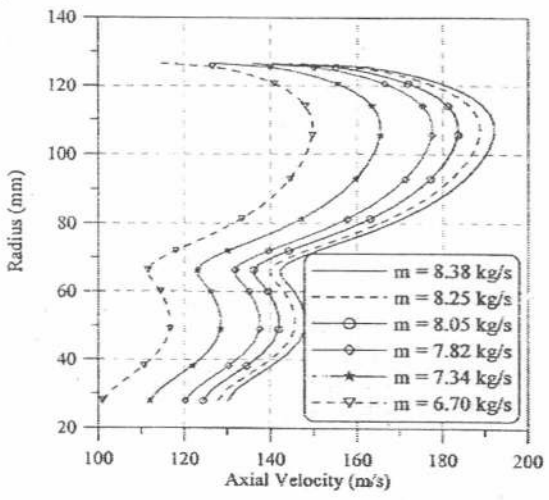

Fig. 13a— Radial variation of axial velocity at the diffuser exit

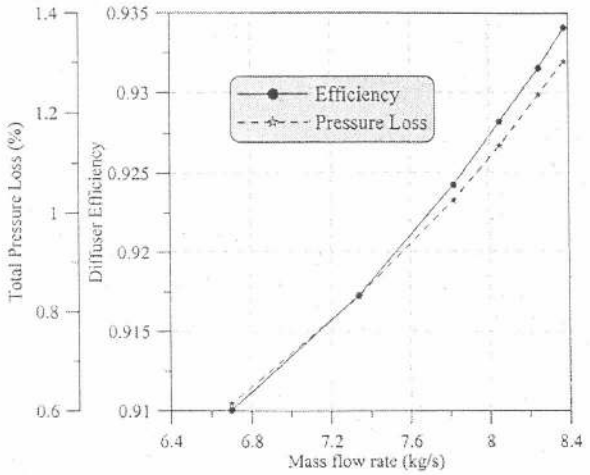

Fig. 13b— Diffuser efficiency and total pressure loss with mass flow rate in the diffuser

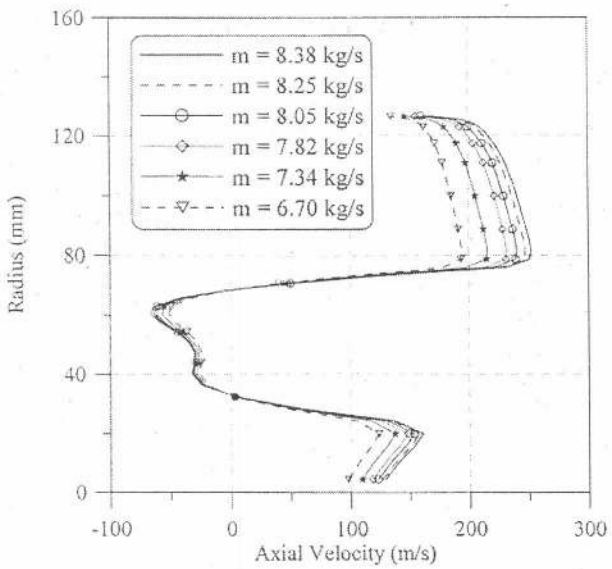

Fig. 13c —Radial variation of axial velocity at $x/r = 1.76$

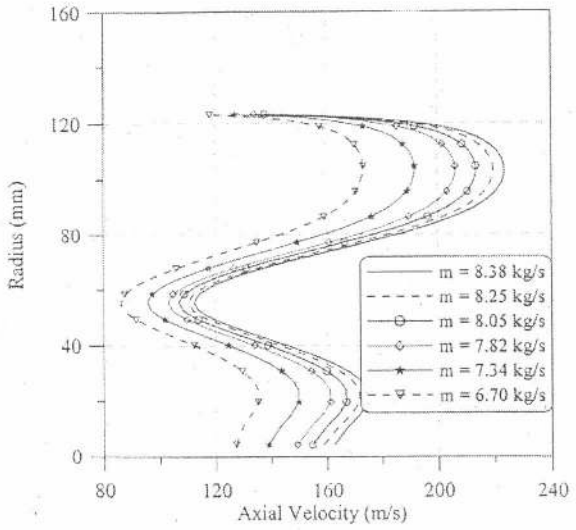

Fig. 13d— Radial variation of axial velocity at $x/r = 2.66$

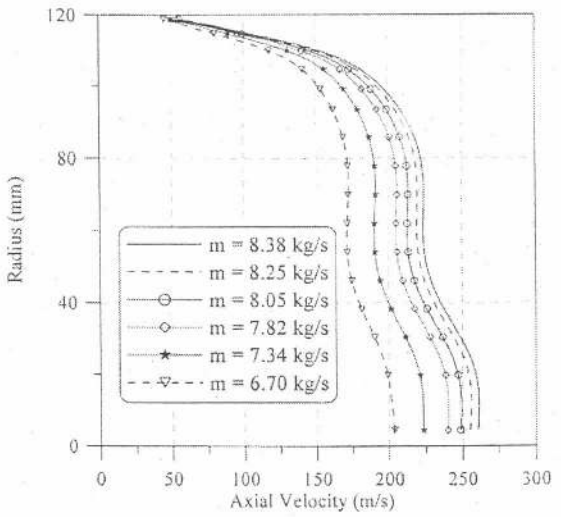

Fig. 13e— Radial variation of axial velocity at $x/r = 4.08$

Fig. 13f shows radial variation of axial velocity at the exit of the nozzle. As expected effect of mass flow rate has reasonable influence over nozzle exit velocity. An increase of 20% in mass flow rate increases the exit nozzle velocity by 35%. Also it may be seen that at the exit the velocity profile is more or less uniform except in the wall region.

Conclusions

In the present study, a detailed three-dimensional numerical prediction of non-reacting flows in an afterburner has been presented. The validation of the code has been carried out in afterburner model geometry. The agreements between the predicted and measured values are reasonably good for the model afterburner geometry. The study is extended to a practical afterburner system. The axial re-circulation length of the lower v-gutter is larger than top v-gutter. This is due to combined effect of diffuser and lower v-gutter. The wall static pressures of core casing and bypass casing are compared with experimental data obtained from rig results. A close agreement is obtained. The effect of mass flow rate on diffuser, v-gutter and nozzle performance has been analyzed. With the increase in mass flow rate from 6.7 kg/s to 8.38 kg/s, a marginal increase in the diffuser efficiency is obtained from 91% to 93.4%. There is no

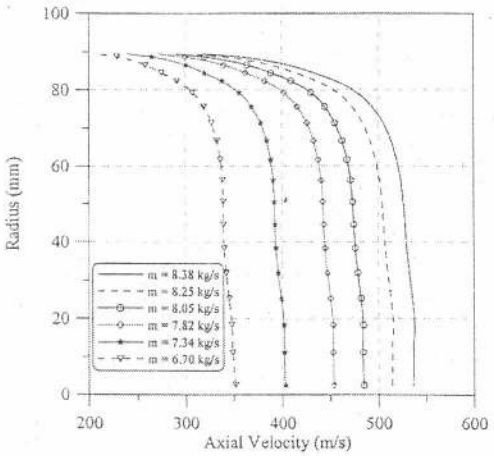

Fig. 13f —Radial variation of axial velocity at exit of the nozzle

change in velocity magnitude in the re-circulation zone with increasing mass flow rate, which indicates the length of the re-circulation is same. Inlet mass flow rate influences the nozzle exit velocity.

Nomenclature

A_1 = core inlet area (m^2)

A_2 = area at the end of diffuser (m^2)

C_p = pressure recovery coefficient

h = static enthalpy (kJ)

$\dot{m}$ = mass flow rate (kg/s)

p = static pressure (Pascal)

p_1 = core inlet static pressure (Pascal)

p_2 = diffuser exit total pressure (Pascal)

p_{01} = core inlet total pressure (Pascal)

r = Radial distance (mm)

U_i = component velocity (m/s)

x_i = component of direction

k = turbulence kinetic energy (m^2/s^2)

ε = turbulent dissipation rate (m^2/s^3)

δ_{ij} = Kronecker-delta

μ = Molecular viscosity (kg/ms)

μ_{eff} = Effective viscosity (kg/ms)

τ_{ij} = Stress tensor

i and j = Indices of the tensorial notation

References

1 Fuji S, Gomi M & Eguchi K, *J Fluids Eng*, 100 (1978) 323-332.

2 Fuji S, Gomi M & Eguchi K, *J Fluids Eng*, 103 (1981) 328-334.

3 Taylor A M K P & Whitelaw J H, *J Fluid Mech*, 139 (1984) 391-416.

4 Yang J T & Tsai G L, *J Fluid Eng*, 115 (1993) 13.

5 Issac J J, Ramesh N R, Rajashekar C, ShyamSundar S R, Baskaran M & Siva Ramakrishna. G, *First Nat Conf on Air Breathing Engines and Aerospace Propulsion*, 1992, pp.221-228,

6 Ravichandran M, *Experimental and theoretical investigations of afterburner*, Ph.D. Thesis, IC Engines Laboratory, Indian Institute of Technology Madras, 1993.

7 Ganesan V, *Indian J Technol*, 18 (1980) 447-450.

8 Vatistas G H, Lin S & Kwok C K, *Bluff body flame holder wakes: A simple numerical solution*, Paper No.AIAA-82-1177, AIAA/SAE/ASME 18th Joint Propulsion Conference, Cleveland, Ohio,1982.

9 Lee D & Lin J S, *Numer Heat Transfer, Pt A*, 20 (1991) 65-79.

10 Raffoul C N, Nejad A S, Gould R D & Spring S A, *J Eng Gas Turbines Power*, 119 (1997) 328-339.

11 *User Guide*, STAR-CD, Version 3.10 A, Computational Dynamics Limited, UK, 1999.